

Supporting Information:

Multi-scale Modeling and Experimental Investigation of Oxidation Behavior in Platinum Nanoparticles

Tom Demeyere,[†] Husn U. Islam,[‡] Tom Ellaby,[‡] Misbah Sarwar,[‡] David
Thompsett,[‡] and Chris-Kriton Skylaris^{*,†}

[†]*School of Chemistry, University of Southampton, Highfield, Southampton SO17 1BJ,
United Kingdom*

[‡]*Johnson Matthey Technology Centre, Blount's Ct, Sonning Common, Reading, United
Kingdom*

E-mail: C.Skylaris@soton.ac.uk

Experimental setup

The three samples of 10, 20, and 50 wt% Pt supported on a carbon black support were synthesized using a procedure adapted from the method disclosed in the patent by Ball et al.^{S1}

X-Ray Diffraction

XRD patterns of the catalysts were obtained using a Bruker D8 diffractometer using Cu $K_{\alpha 2}$ radiation. The diffraction patterns were analyzed using Reitfeld analysis to calculate crystallite sizes and lattice parameters. However, crystallite sizes below 2 nm were not determined due to the broadness and poor quantity of the data.

Transmission Electron Microscopy

TEM images of the catalysts were obtained using a JEM 2800 scanning TEM using a voltage of 200kV. Particle size distributions were determined using dark field images.

Extended X-ray Absorption Fine Structure

The X-ray absorption spectra of the Pt L3 (11.5634 KeV) edge were collected at beamline B18 at the Diamond Light Source, UK. Data was collected in transmission, using a Si(111) monochromator, and calibrated to a Pt foil reference. Before measurements, samples were pressed into 13 mm pellets. References were diluted with cellulose before pelleting. Pt foil, platinumic acid ($H_2Pt(OH)_6$), and Pt acetylacetonate were used as references for Pt^0 , Pt^{4+} , and Pt^{2+} respectively. The data was analyzed using Athena and Artemis from the Demeter suite of software. X-ray absorption near edge structure (XANES) was fitted using linear combination fitting (LCF) analysis with the references, and extended X-ray fine structure (EXAFS) was fitted using the EXAFS equation with Pt-O and Pt-Pt interatomic distances.

Computational Details

ReaxFF Monte Carlo and Molecular Dynamics

For these simulations, we used the 2 Aug. 2023 version of the Large-scale Atomic/Molecular Massively Parallel Simulator (LAMMPS) software.^{S2} Our Monte-Carlo approach is based on the Hybrid MD-MC scheme,^{S3} where a subset \mathcal{A} of the total system still samples the canonical ensemble, while particles belonging to the subset \mathcal{B} are sampled in the grand canonical ensemble, i.e. being added or removed. The resulting ensemble cannot be written as the product of the two ensembles:

$$\mathcal{Z}_{AB} \neq Z_A \Xi_B \quad (1)$$

Where \mathcal{Z} is the total partition function, Z_A is the partition function of the canonical ensemble and Ξ_B is the partition function of the grand canonical ensemble. The inequality arises from the strong interaction between the two subsystem for which clearly $E_{AB} \neq E_A + E_B$ due to the important excess energy of interaction. Instead, the resulting ensemble is called "semi-grand canonical".^{S4} We note that the use of the term 'semi-grand canonical' refers to a system where one sub-system is treated in the grand canonical ensemble and another sub-system in the canonical ensemble, following the terminology used by Vafaei et al.^{S4} This differs from other implementations where 'semi-grand canonical' refers to simulations with a fixed total number of atoms where only the relative amounts of each species can vary.

To derive the partition function of the ensemble we first write the partition function of the canonical ensemble:

$$Z(N_A, N_B, V, T) = \frac{1}{\Lambda_A^{3N_A} N_A! \Lambda_B^{3N_B} N_B!} \int d\mathbf{r}_A^{N_A} d\mathbf{r}_B^{N_B} e^{-\beta U(\mathbf{r}_A^{N_A}, \mathbf{r}_B^{N_B})} \quad (2)$$

The semi-grand canonical partition is then found by performing a discrete Laplace transformation of the canonical partition function, summing over N_B and therefore conceptually

removing the dependence on N_B , in favor of the conjugate variable μ_B .^{S4}

$$\tilde{\Xi}(N_A, \mu_B, V, T) = \sum_{N_B} e^{\beta \mu_B N_B} Z(N_A, N_B, V, T) \quad (3)$$

The semi-grand canonical ensemble is then defined by the chemical potential $\mu_B \equiv \mu$, the temperature T , the volume V , and the fixed number of atoms N_A of subset \mathcal{A} . In practice, we perform 50 additions/deletions and 100 displacement moves every 5 MD timestep. These numbers have to be correctly chosen to ensure that the system can explore the phase space efficiently and to avoid specific regions of the system being stuck in local minima due to the lack of displacement move and MD moves. The maximum displacement distances for displacement move is set to 0.05 Å. Such small displacements are chosen because atomic oxygen often bind strongly to one specific site, and large displacement will often result in high rejection rates. We also should note that as the platinum atoms are moving, such small displacements with higher acceptance rate, will allow the oxygen atoms to follow platinum dynamics more effectively. The MD timestep is chosen as 0.25 fs.

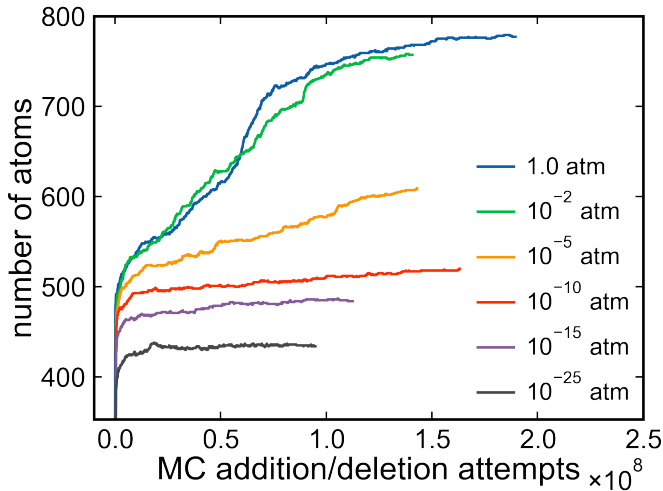


Figure S1: Total number of atoms vs. exchange moves for the various pressures under study. Clear convergence are observed for low pressures, but not for higher pressures where the system is not able to reach equilibrium.

The temperature of both canonical and grand canonical ensemble is set to 350 K. At any time, the Nosé-Hoover canonical thermostat has to be updated to reflect the new number of

degrees of freedom due to the addition or deletion of particles in subset \mathcal{B} . This is done in LAMMPS by using the *compute_modify* command. Finally, we impose a minimum distance of 0.8 Å with every other atom when adding a particle to the system. This limitation is needed because ReaxFF potentials often have complex and non-smooth potential energy surfaces, which can lead to numerical instability if atoms are too close to each other. This is achieved by using the *overlap_cutoff* option in the *fix gcmc* command of LAMMPS. This option allows the user to set a minimum distance between atoms when, displacing, adding or deleting particles. This is done by attributing a large positive energy penalty to configurations where atoms are too close to each other. As a result, the Monte Carlo algorithm will reject moves that lead to such configurations, and accept deletion moves to move away from them. Using such option, we did not encounter situations where the system would find itself in an artificial local minimum with atoms too close to each other. Before running the MC-MD simulations, we perform a geometry optimization of the system using the ReaxFF potential with the LAMMPS software using the *minimize* command. The energy threshold is set to 10^{-6} kcal/mol, and the maximum number of iterations is set to 10^4 . The system is then shortly equilibrated for 1 ps in the canonical ensemble before starting the MC moves. For the second step of the workflow, we continue the dynamics of our systems by stopping the grand canonical Monte-Carlo moves, other specific parameters are kept the same as previously.

Figure S1 clearly shows the difficulty associated with the convergence of the MC-MD simulations at high pressures. Such difficulties are notorious with Monte Carlo methods, where techniques to increase acceptance rates (biased moves, parallel tempering, energy minimization schemes) are therefore commonly used. In our case, the platinum nanoparticle undergoes continuous dynamic changes during the simulation. This constant flux of configurations creates a highly variable environment for Monte Carlo moves. This constantly evolving behavior periodically creates configurations that are more favorable for addition or deletion moves. This results in sudden increases or decreases in the total number of atoms,

which provoke sharp fluctuations in the convergence plot. As stated in the main text, because the aim of the study is not necessarily to reach an equilibrium of the system, but rather to observe the effect of increasing oxygen coverage, we are satisfied with the current results.

MACE-MP-0

Calculations with the MACE-MP-0 potential have been performed using the "mace" code available at <https://github.com/ACEsuit/mace>^{S5} we used the *large* (MPtrj) foundation model trained on the Material Project database consisting of approximately 146,000 unique crystal structures.^{S6} No dispersion correction is used, and the model is run using the float64 precision. The geometry optimizations have been done using the *BFGSLineSearch* from the Atomic Simulation Environment^{S7} (ASE) package (3.22.0) with a maximum force criteria of 0.01 eV/Å.

ONETEP calculations

ONETEP (Order-N Electronic Total Energy Package) is a quantum chemistry software implementing linear-scaling density functional theory (DFT). Its efficiency for large systems stems from using localized Non-orthogonal Generalized Wannier functions (NGWFs) as its basis. These NGWFs are transformations of the Kohn-Sham orbitals and are expressed in terms of a psinc (periodic sinc) basis set, which is related to plane waves via a unitary transformation. ONETEP solves the electronic structure problem through a sparse density matrix approach, combining NGWFs with a density kernel which is a projection of the occupancies on the NGWF orbitals. The software employs a dual minimization method, optimizing both NGWFs and the density kernel for an accurate description of the electronic structure. This framework allows ONETEP to combine the advantages of localized functions for linear scaling with the accuracy of plane waves, making it particularly effective for large, complex systems where traditional cubic-scaling DFT methods become impractical.

The core electrons are described using norm-conserving pseudopotentials from the ONCV library. The Perdew-Burke-Ernzerhof (PBE) exchange-correlation functional is employed for the calculations. Ensemble Density Functional Theory (EDFT) calculations are performed with an EDFT smearing width of 700.00 K. To adequately represent the Platinum (Pt) and Oxygen (O) atoms, we use 13 NGWFs for Pt and 4 NGWFs for O. NGWF radius are set to 12.0 Bohr. The calculations are performed with spin polarization activated. The energy cutoff which dictates the psinc grid spacing is set to 32 Ha. The energy criterion is set to 5×10^{-6} Ha for the NGWF RMS gradient and 10^{-3} Ha for the total energy. For more information about ONETEP, the reader is redirected to the main paper.^{S8}

References

- (S1) Ball, S. C.; Hards, G. A.; Rodlert, M.; Sharman, J. D. B.; Spahr, M. E. Carbon Supported Catalyst. 2017.
- (S2) Thompson, A. P.; Aktulga, H. M.; Berger, R.; Bolintineanu, D. S.; Brown, W. M.; Crozier, P. S.; in 't Veld, P. J.; Kohlmeyer, A.; Moore, S. G.; Nguyen, T. D.; Shan, R.; Stevens, M. J.; Tranchida, J.; Trott, C.; Plimpton, S. J. LAMMPS - a Flexible Simulation Tool for Particle-Based Materials Modeling at the Atomic, Meso, and Continuum Scales. *Computer Physics Communications* **2022**, *271*, 108171.
- (S3) Frenkel, D.; Smit, B. *Understanding Molecular Simulation: From Algorithms to Applications*, 2nd ed.; Computational Science Series 1; Academic Press: San Diego, 2002.
- (S4) Vafaei, S.; Tomberli, B.; Gray, C. G. McMillan-Mayer Theory of Solutions Revisited: Simplifications and Extensions. *The Journal of Chemical Physics* **2014**, *141*, 154501.
- (S5) Batatia, I.; Kovács, D. P.; Simm, G. N. C.; Ortner, C.; Csányi, G. MACE: Higher Order Equivariant Message Passing Neural Networks for Fast and Accurate Force Fields. 2023.

- (S6) Batatia, I.; Benner, P.; Chiang, Y.; Elena, A. M.; Kovács, D. P.; Riebesell, J.; Advincula, X. R.; Asta, M.; Avaylon, M.; Baldwin, W. J.; Berger, F.; Bernstein, N.; Bhowmik, A.; Blau, S. M.; Cărare, V.; Darby, J. P.; De, S.; Della Pia, F.; Deringer, V. L.; Elijošius, R.; El-Machachi, Z.; Falcioni, F.; Fako, E.; Ferrari, A. C.; Genreith-Schriever, A.; George, J.; Goodall, R. E. A.; Grey, C. P.; Grigorev, P.; Han, S.; Handley, W.; Heenen, H. H.; Hermansson, K.; Holm, C.; Jaafar, J.; Hofmann, S.; Jakob, K. S.; Jung, H.; Kapil, V.; Kaplan, A. D.; Karimitari, N.; Kermode, J. R.; Kroupa, N.; Kullgren, J.; Kuner, M. C.; Kuryla, D.; Liepuoniute, G.; Margraf, J. T.; Magdău, I.-B.; Michaelides, A.; Moore, J. H.; Naik, A. A.; Niblett, S. P.; Norwood, S. W.; O'Neill, N.; Ortner, C.; Persson, K. A.; Reuter, K.; Rosen, A. S.; Schaaf, L. L.; Schran, C.; Shi, B. X.; Sivonxay, E.; Stenczel, T. K.; Svahn, V.; Sutton, C.; Swinburne, T. D.; Tilly, J.; van der Oord, C.; Varga-Umbrich, E.; Vegge, T.; Vondrák, M.; Wang, Y.; Witt, W. C.; Zills, F.; Csányi, G. A Foundation Model for Atomistic Materials Chemistry. 2024.
- (S7) Larsen, A. H.; Mortensen, J. J.; Blomqvist, J.; Castelli, I. E.; Christensen, R.; Duřak, M.; Friis, J.; Groves, M. N.; Hammer, B.; Hargus, C.; Hermes, E. D.; Jennings, P. C.; Jensen, P. B.; Kermode, J.; Kitchin, J. R.; Kolsbjerg, E. L.; Kubal, J.; Kaasbjerg, K.; Lysgaard, S.; Maronsson, J. B.; Maxson, T.; Olsen, T.; Pastewka, L.; Peterson, A.; Rostgaard, C.; Schiøtz, J.; Schütt, O.; Strange, M.; Thygesen, K. S.; Vegge, T.; Vilhelmsen, L.; Walter, M.; Zeng, Z.; Jacobsen, K. W. The atomic simulation environment—a Python library for working with atoms. *Journal of Physics: Condensed Matter* **2017**, *29*, 273002.
- (S8) Prentice, J. C. A.; Aarons, J.; Womack, J. C.; Allen, A. E. A.; Andrinopoulos, L.; Anton, L.; Bell, R. A.; Bhandari, A.; Bramley, G. A.; Charlton, R. J.; Clements, R. J.; Cole, D. J.; Constantinescu, G.; Corsetti, F.; Dubois, S. M.-M.; Duff, K. K. B.; Escartín, J. M.; Greco, A.; Hill, Q.; Lee, L. P.; Linscott, E.; O'Regan, D. D.; Phipps, M.

J. S.; Ratcliff, L. E.; Serrano, Á. R.; Tait, E. W.; Teobaldi, G.; Vitale, V.; Yeung, N.; Zuehlsdorff, T. J.; Dziedzic, J.; Haynes, P. D.; Hine, N. D. M.; Mostofi, A. A.; Payne, M. C.; Skylaris, C.-K. The ONETEP Linear-Scaling Density Functional Theory Program. *The Journal of Chemical Physics* **2020**, *152*, 174111.